Full Paper

Propellants, Explosives, Pyrotechnics

DOI: 10.1002/prep.201900164

Detonation Characteristics of an Aluminized Explosive Added with Boron and Magnesium Hydride

Wei Cao,[a] Qingguan Song,[a] Dayuan Gao,[a] Yong Han,*[a] Sen Xu,[b] Xiaojun Lu,[a] and Xiangli Guo*[a]

Abstract: Investigation of the detonation characteristics of an aluminized explosive added with boron (B) and magnesium hydride (MgH_2) were undertaken and compared with the aluminized explosive of similar formulation. Firstly, the explosion heat was measured in a vacuumed calorimetric bomb, then the detonation pressure was determined by the interface velocity experiment, and finally the cylinder expansion test was performed. From the calorimetric data, the addition of B and MgH_2 into an aluminized explosive increases the heat of explosion slightly. From the detonation pressure data, the addition of B and MgH_2 appears to have no significant influence to the detonation pressure. From the cylinder test data, the detonation velocity, wall velocity, Gurney energy and detonation energy were determined. The aluminized explosive added with B and MgH_2 shows weak acceleration ability, but exhibits a stronger afterburning potential. Finally the equation of state of the detonation products was determined for different casing conditions. Conclusions about how to use B and MgH_2 in aluminized explosives to generate optimal effects are drawn.

Keywords: detonation characteristics · aluminized explosive · boron · magnesium hydride · cylinder test

1 Introduction

Aluminum (Al) has been added to explosives since the beginning of 20th century [1], currently it is still widely used as a metal additive in explosives and propellants due to its high calorific value, which can increase reaction temperature, blast and incendiary effects. Compared with aluminum, boron (B) has a higher calorific value, no matter gravimetric heat of combustion or volumetric heat of combustion [2]. Therefore, boron seems to be a potential fuel additive in energetic materials. Nevertheless, experimental effort indicated that the difficulties of ignition and combustion of boron are obstacles to its application [3]. In part, this is due to the extremely high melting and boiling temperatures of boron at 2450 and 3931 K, and the formation of a liquid boron oxide (B_2O_3) layer with a relatively high boiling point of 2316 K on the boron particle surface, which reduces the ability of the fuel to mix with oxidizer and leads to inefficient burning [4].

Nonetheless, some studies relating to boron utilization in explosives were reported recently. Makhov [5] introduced powdered boron and aluminum into high explosives individually and compared the heat of explosion and acceleration ability of them, results show that aluminized compositions are superior to boron-containing mixtures in these parameters. Xu et al. [6] measured the heat of combustion of Al/B powder and underwater explosion parameters of metallized explosives containing aluminum and boron powders. It shows that the addition of aluminum powder increases the combustion efficiency of boron, and the combustion efficiency of boron decreases with increasing boron content in the mixture. The metallized explosive (RDX/ammonium perchlorate (AP)/metal powder/binder = 36/20/35/9) containing metal powder of Al/B = 90/10 has the highest bubble energy and total useful energy. Chen et al. [7] measured the underwater explosion parameters of explosive mixtures (RDX/AP/metal powder/binder = 36/20/35/9) containing a novel hydrogen storage alloy (Al/B/MgH_2 = 70/10/20) as the metal powder, results show that the RDX-based explosive enriched novel hydrogen storage alloy can produce a slightly higher bubble energy and total energy than similar formulated RDX-based explosive enriched Al.

Above review of the literature shows that the addition of B and MgH_2 into aluminized explosives seems to improve the energy output of explosives. It appears that the combustion heat of Al and MgH_2 can enhance the combustion efficiency of B. Besides, the combustion of MgH_2 generates H_2O, which can improve the ignition and combustion of B [8, 9]. What needs to be specified is that metal hydride materials (especially light metal hydride materials) are also po-

[a] *W. Cao, Q. Song, D. Gao, Y. Han, X. Lu, X. Guo*
Institute of Chemical Materials, China Academy of Engineering Physics
P.O. Box 919–319, Mianyang, Sichuan 621999, P.R. China
**e-mail: y_han76@126.com*
guoxl@caep.cn
[b] *S. Xu*
School of Chemical Engineering, Nanjing University of Science and Technology
No.200 Xiaolingwei Street, Nanjing, Jiangsu 210094, P.R. China

 © 2019 Wiley-VCH Verlag GmbH & Co. KGaA, Weinheim

tential energetic materials, since they can store a large amount of hydrogen and release high heat of combustion [10]. The addition of metal hydride materials into explosives has also been investigated by many researchers recently. For instance, the detonation properties of ammonium nitrate (AN)/RDX/TNT with AlH_3/MgH_2 [11], the explosion properties of RDX with MgH_2/TiH_2 [12–14] and emulsion explosives with MgH_2/TiH_2 [15–17], the detonation heat and confined explosion parameters of RDX with TiH_2/ZrH_2 [18, 19], the mechanical sensitivity of AN/TNT/RDX with $MgH_2/Mg(BH_4)_2$ [20], and the thermal behaviors of TNT with $MgH_2/Mg(BH_4)_2$ [21] and TNT/RDX with $Mg(BH_4)_2$ [22] were reported.

The objective of the present work is to determine the detonation characteristics of a novel aluminized explosive added with B and MgH_2 to explore what role of B and MgH_2 play in the detonation reaction. The characteristics include calorimetric heat of detonation, detonation pressure, Gurney energy, detonation energy and Jones-Wilkins-Lee (JWL) equation of state (EOS). The obtained parameters are also compared with those of a similar formulated aluminized explosive to get ideas about the potential use of the aluminized explosive added with B and MgH_2.

2 Explosive Samples Preparation

Explosive mixtures were granulated form RDX (36 wt.%, average particle size $D_{50}=30$ μm, Gansu Yinguang Chemical Industry Group Co., Ltd., China), AP (NH_4ClO_4, 20 wt.%, $D_{50}=$ 40 μm, Norinco Group Hubei Dongfang Chemical Industry Co., Ltd., China), metal powders (35 % wt.%), and others (9 wt.%, including wax, graphite, and binder). Metal powders used in this work are spherical pure aluminum ($D_{50}=$ 2 μm, Angang Group Aluminum Powder Co., Ltd., China) and irregular novel alloy of aluminum, boron and magnesium hydride ($Al/B/MgH_2=70/15/15$, $D_{50}=3$ μm, Institute of Metal Research, Chinese Academy of Science, China), respectively. Thus two explosive formulations enriched aluminum and alloy were prepared and named as AL and BH with oxygen balance of −0.622 and −0.709, respectively. The morphology of aluminum and alloy were observed by scanning electron microscopy (SEM) and illustrated in Figure 1. Various dimensional cylindrical charges were pressed for different tests, and the densities ρ_0 of AL and BH are 1.85 and 1.77 (±0.005) g/cm^3, respectively.

3 Calorimetric Heat of Explosion

The calorimetric heat of explosion (Q_c) of the tested composites was measured according to the method described in [23]. The cylindrical bomb, made of stainless steel, has a volume of 5.0 L. A cylindrical charge with mass of 25 g and diameter 20 mm was initiated by a standard fuse (5 g PETN booster with $\rho_0=1.60\pm0.005$ g/cm^3 and No. 8 detonator) in vacuum atmosphere. To calculate the detonation heat of sample charge, the measured total heat is subtracted by the heat released from the fuse. At least two measurements were performed for each explosive. The calorimetric heat of explosion of AL and BH is determined as 7480 (±20) and 7590 (±20) kJ/kg, respectively. BH has a slightly higher heat value of explosion, which indicates the superiority of the alloy.

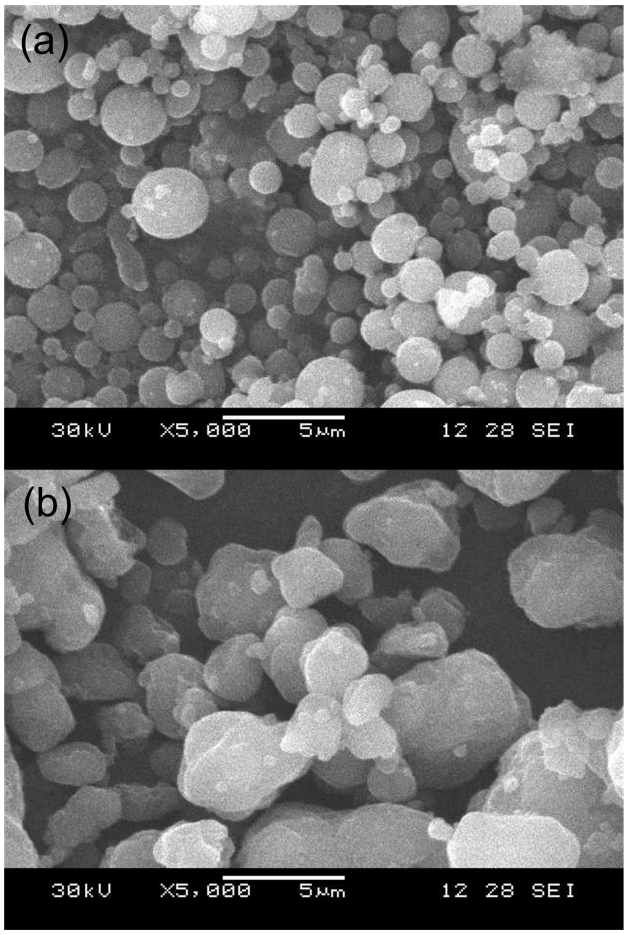

Figure 1. SEM images of aluminum powders (a) and alloy powders (b).

4 Detonation Pressure

The detonation pressure was calculated from the interface velocity experiment, in which the interface particle velocity histories between detonating explosives and LiF transparent windows were recorded by a photonic Doppler velocimetry (PDV) system with nanosecond time scales [24]. A Φ50 mm × 45 mm cylindrical sample charge was detonated by a plane wave lens at one end and a Φ 20 mm × 10 mm LiF window was mounted at the center of the other end. A 0.6-μm-thick aluminum foil was deposited on the window

 © 2019 Wiley-VCH Verlag GmbH & Co. KGaA, Weinheim

face next to the explosive to provide a reflective surface. The aluminum layer is thin enough (< 1 μm) and has a shock impedance close to that of LiF window to introduce negligible perturbations into the flow and interface velocity histories. Figure 2 illustrates the experimental geometry of the interface velocity measurement.

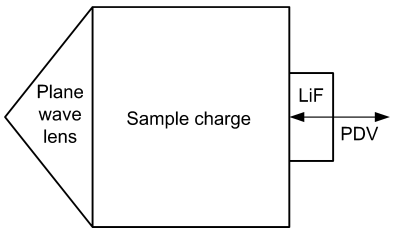

Figure 2. Geometry of the interface velocity measurement.

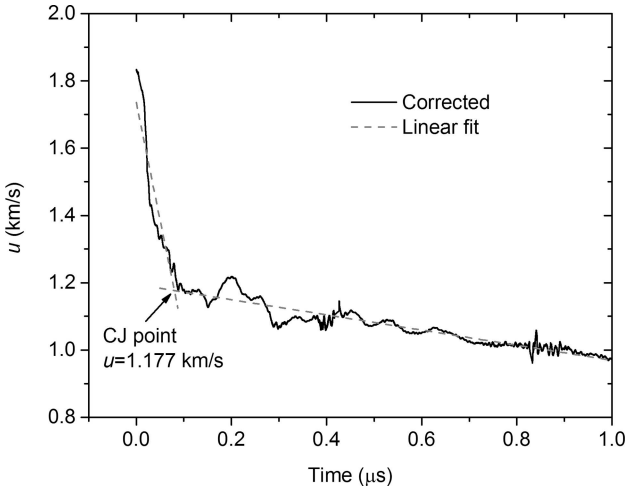

Figure 3. Interface particle velocity histories of BH.

Apparent interface velocity histories are obtained and corrected for the index of refraction of LiF to generate true interface velocity histories [25]. Now we just focused on the corrected velocity profiles. For both the explosives the Zeldovich-von Neumann-Doering (ZND) detonation wave structure was observed: a discontinuous jump to maximum particle velocity at the detonation wave front followed by a decrease to the Chapman-Jouguet (CJ) velocity as the chemical energy is released. The plot consists of two straight lines corresponding to different laws of shock attenuation [26]: a nonreactive shock followed by a steady-state reaction zone which is terminated at the CJ surface where the local flow velocity plus sound speed equals the detonation velocity, and an unsteady flow behind the CJ plane which may be simply described as a rarefaction wave ending in cavitation or in a steady-state region required to match boundary conditions at the back boundary of the explosive products. The corrected interface velocity and two linear fit lines for BH were drawn in Figure 3. The point of their intersection was associated with the CJ point. Thus, the CJ particle velocity u_{CJ} is determined as 1.165 and 1.177 km/s for AL and BH.

LiF is an inert material with a higher shock impedance than the main charge, thus a strong shock is reflected back into the reacting explosive. We can do impedance analysis on the measured point at the explosive-window interface. Using the linear Hugoniot relation of LiF, which is established from the experimental relation of shock velocity U_s and particle velocity u as [27]

$$U_s = 5.201 + 1.323u. \quad (1)$$

The impedance match equation was then used to calculate the incident or detonation pressure [28]. The impedance equation is

$$P_i = u(\rho_{LiF}U_s + \rho_0 D)/2, \quad (2)$$

where P_i is the incident or detonation pressure, ρ_{LiF} the initial density of LiF (2.64 g/cm^3), D the detonation velocity of the explosive which will be given in next section, ρ_0 the initial density of the explosive. By using Equation (1) and (2) with $u = u_{CJ}$, the CJ detonation pressure $P_{CJ} = P_i$ is calculated to be 17.8 and 17.5 GPa for AL and BH. The measurement uncertainty was ~3%, which results from the accuracy of determining the CJ point, the correction of interface velocity and the Hugoniot relation of LiF.

5 Cylinder Test

The cylinder test was performed to determine the acceleration ability and energetic characteristics for samples AL and BH. During each test, twelve cylindrical pressed charges with dimension of Φ25 mm × 25 mm were inserted into 300 mm long, 25 mm inner diameter, and 30 mm outer diameter copper tube (oxygen free copper). A Φ25 mm × 25 mm booster (HMX/binder = 95/5, $\rho_0 = 1.857 \pm 0.002$ g/cm^3) was used to initiate the explosive at one end. The radial motion of the cylinder wall was measured in a plane perpendicular to the cylinder axis 200 mm form the booster end. A high-speed rotating mirror streak camera (writing speed 1.5 mm/μs) recorded the motion, using an argon bomb as an illuminator. A typical photograph of the copper tube driven by the detonation products of BH is shown in Figure 4.

5.1 Detonation Velocity

The experimental detonation velocity D of explosives were measured simultaneously during the cylinder test using the

 © 2019 Wiley-VCH Verlag GmbH & Co. KGaA, Weinheim

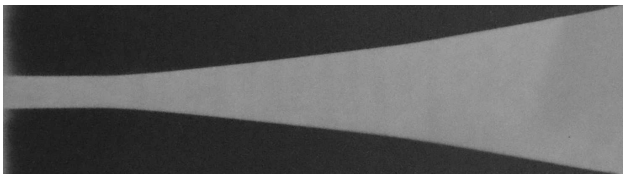

Figure 4. Photograph of the copper tube driven by the detonation products of BH.

short-circuit sensors method [29]. Thus, the detonation velocity was obtained as 6860 and 6730 m/s for AL and BH, respectively. The measurement uncertainty was ~1 %, mainly originating from the accuracy of measuring the distance between the sensors.

5.2 Tube Velocity and Acceleration Ability

Details of the procedure for determining the tube velocity form the cylinder test results are given in [30]. Firstly, the central cylinder surface r_m, which halves the surface of the cylinder cross-section, is determined from the tube profile by assuming a complete incompressibility of the tube material. Meanwhile, assuming that the motion of the detonation products and the tube material could be treated as a stationary one (which means that $x = D \bullet t$, where t is time), the dependence of r_m on the axis coordinate can be changed to the dependence of time. The time dependence of the position of the tube's central surface is approximated by an appropriate function. The radial velocity of the tube (u_m) can then be calculated by differentiating this function and finally the total velocity (u_L) is expressed by the following equation:

$$u_L = 2D\sin(\theta/2),\ \theta = \mathrm{arctg}(u_m/D). \tag{3}$$

Applying the experimental profiles of the outer surface radius of the tube on the axial coordinate constructed form the photograph (Figure 4) and the detonation velocities (section 5.1), the dependence of u_L on the relative volume of the detonation products is plotted in Figure 5.

The acceleration ability of an explosive can be described by the so-called Gurney energy E_G, which is defined as a sum of the kinetic energy of the expanding detonation products and displaced walls materials [31]. For cylindrical geometries, the Gurney energy is expressed as

$$E_G = (\mu + 1/2){u_L}^2/2, \tag{4}$$

where μ is the ratio between the cylinder and the explosive per unit of length. The obtained results are presented in Figure 6.

Practically, these final values of the wall velocity and Gurney energy before the disruption of the copper tube are the most important. From Figure 5 and 6, the profiles exhibit similar trends. At the initial expanding process, the copper tube driven by AL accelerates faster than BH. With increasing relative volume of detonation products (3 and more), the velocity difference between AL and BH decreases. These indicate that, compared with pure aluminum, the reaction of the alloy is more difficult after initiation, but can release more energy in the later expanding process. In addition, the profiles continue to rise and do not reach a plateau (unlike TNT and phlegmatized RDX in [32]) during the relative volume of nine permitted by the cylinder test, which indicates a remained amount of energy is still stored in the detonation products. Values of the copper tube velocity and Gurney energy at a relative tube volume of nine are listed in Table 1.

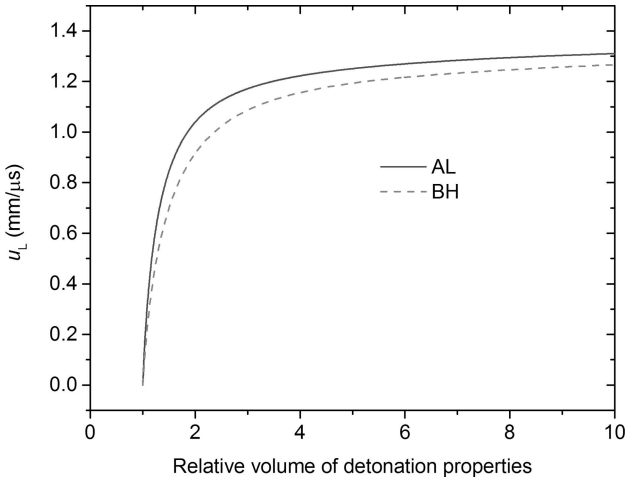

Figure 5. Variation of the tube wall total velocity with the relative volume of detonation products.

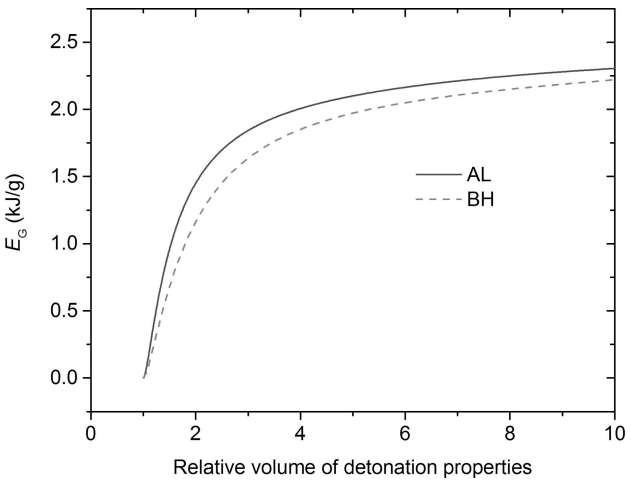

Figure 6. Variation of the Gurney energy with the relative volume of detonation products.

 © 2019 Wiley-VCH Verlag GmbH & Co. KGaA, Weinheim

Table 1. Copper tube total velocity and Gurney energy.

Explosive	u_L (m/s)	E_G (kJ/kg)
AL	1303	2312
BH	1273	2205

5.3 Detonation Energy

The detonation energy e_0 of the explosives, which is defined as the maximum work done by the detonation products during their expansion from the CJ point to infinite volume minus the compression energy [32], can be calculated from the cylinder test results by the method described in [33]. As was shown in [33], a relationship between the detonation energy and the tube kinetic energy is

$$\frac{e^0}{e_0^{st}} = \frac{\mu + 1/2}{\mu^{st} + 1/2}\left(\frac{u_L}{u_L^{st}}\right)^2, \tag{5}$$

where e_0 and $e_0{}^{st}$ present the detonation energy per unit mass of the tested explosive and a standard (reference) explosive, respectively, and u_L and $u_L{}^{st}$ are the velocities of the expanded tubes at a relative volume of 9. In order to determine the detonation energy of the explosives, a standard explosive of TNT was chosen. Its energy of detonation 4430 kJ/kg for a density of 1.60 g/cm^3 and $u_L{}^{st} = 1402$ m/s was chosen from [32]. Thus, e_0 for AL and BH is estimated as 3396 and 3275 kJ/kg, respectively.

A comparison of the detonation energy results with the calorimetric explosion heats of the explosives draws a conclusion, that considerable amount of energy is still reserved in the detonation products till the relative volume of nine permitted by the cylinder test, this is why the Gurney energy of the explosives continues to rise and does no reach a plateau. These results are in accordance with [32].

5.4 JWL EOS

The equation known as the JWL EOS for the isentropic expansion of the detonation products of condensed explosives has the following form [34]:

$$P = A\left(1 - \frac{\omega}{R_1 V}\right)e^{-R_1 V} + B\left(1 - \frac{\omega}{R_2 V}\right)e^{-R_2 V} + \frac{\omega E_0}{V}, \tag{6}$$

where P denotes the pressure, GPa; V is the relative specific volume; A, B, R_1, R_2 and ω are constants for a given explosive, E_0 is the initial energy per unit volume of explosives, J/mm^3. The corresponding JWL isentrope is expressed as [34]:

$$P = Ae^{-R_1 V} + Be^{-R_2 V} + CV^{-(\omega+1)}, \tag{7}$$

Cylinder test data are commonly employed in most methods for the determination of the JWL coefficients. For the CJ point (variants are denoted by subscript CJ), the connections between the JWL coefficients following from the conservation laws are expressed as [30]

$$AR_1 e^{-R_1 V_{CJ}} + BR_2 e^{-R_2 V_{CJ}} + C(\omega + 1)V_{CJ}^{-(\omega+2)} = \rho_0 D_{CJ}^2, \tag{8}$$

$$\frac{A}{R_1}e^{-R_1 V_{CJ}} + \frac{B}{R_2}e^{-R_2 V_{CJ}} + \frac{C}{\omega}V_{CJ}^{-\omega} = E_0 + \frac{1}{2}P_{CJ}(1 - V_{CJ}), \tag{9}$$

$$Ae^{-R_1 V_{CJ}} + Be^{-R_2 V_{CJ}} + CV_{CJ}^{-(\omega+1)} = P_{CJ}, \tag{10}$$

where $V_{CJ} = k/(k+1), k = \rho_0 D_{CJ}^2/P_{CJ} - 1$.

Thus, the parameters A, B and C are expressed as functions of R_1, R_2, ω, the density of the explosive ρ_0, the detonation velocity D, the detonation pressure P_{CJ}. The initial values of R_1, R_2 and ω were chosen from the known JWL coefficients for other aluminized explosive, then values of A, B and C were obtained from Eqs. (8–10). A two-dimensional axisymmetric Lagrange cylinder test model was established according to the dimensions of cylinder test by hydrocode LS-DYNA. Material models of *MAT_HIGH_EXPLOSIVE BURN and *MAT_JOHNSON_COOK, and EOS of *EOS_JWL and *EOS_GRUNEISEN were chosen for the explosive and copper, respectively [35].The numerical simulation of the tube radius on the axial coordinate is compared with that obtained from experiment. This procedure is repeated with adjusted values of R_1, R_2 and ω until the difference between the experimental and numerical results becomes small enough. Two sets of JWL isentrope were obtained for each explosive. The first one was calculated using the value of the detonation energy determined from the cylinder test results $E_0 = \rho_0 e_0$ (minimum additional energy from the afterburning of metal powders in the detonation products). The second set was determined by using the energy $E_0 = \rho_0 Q_c$ (maximum additional energy). Note that the choice of E_0 is just a basis for energy calculation, what we care about is the effect of the effective working capacity of detonation energy to the coefficients of JWL EOS, thus whether the value of E_0 is accurate is not vital to the true energy output of the explosive reaction. The necessary detonation parameters and the calculated JWL EOS constants are summarized in Table 2. Exemplary results of the simulation to determine JWL EOS constants for E_0 equal to the detonation energy for the explosive BH are presented in Figure 7.

The determined JWL EOS and isentrope for the detonation products of these explosives can be used for modeling and simulation of the processes associated with the detonation of charges made from these compositions. In practice, the degree of the metal powders reaction with the detonation products depends on the casing [36]. As suggested by Maiz and Trzciński [32], the JWL EOS determined using the detonation energy estimated from the cylinder test should properly describe the behavior of the deto-

 © 2019 Wiley-VCH Verlag GmbH & Co. KGaA, Weinheim

Table 2. Calculated JWL EOS constants.

Ex	Detonation parameters	JWL parameters	
AL	$\rho_0 = 1.85$ g/cm^3	$E_0 = \rho_0 e_0 = 6.282$ GPa	$E_0 = \rho_0 Q_c = 13.838$ GPa
	$P_{CJ} = 17.8$ GPa	$R_1 = 6.05$ A $= 1692.4$ GPa	$R_1 = 5.96$ A $= 1570.9$ GPa
	$D = 6860$ m/s	$R_2 = 0.93$ B $= 7.4297$ GPa	$R_2 = 1.35$ B $= 7.6942$ GPa
	$e_0 = 3396$ kJ/kg	$\omega = 0.20$ C $= 0.3854$ GPa	$\omega = 0.08$ C $= 0.8764$ GPa
	$Q_c = 7480$ kJ/kg		
BH	$\rho_0 = 1.77$ g/cm^3	$E_0 = \rho_0 e_0 = 5.797$ GPa	$E_0 = \rho_0 Q_c = 13.434$ GPa
	$P_{CJ} = 17.5$ GPa	$R_1 = 5.83$ A $= 1200.3$ GPa	$R_1 = 5.38$ A $= 938.1$ GPa
	$D = 6730$ m/s	$R_2 = 1.32$ B $= 11.2551$ GPa	$R_2 = 1.38$ B $= 5.6265$ GPa
	$e_0 = 3275$ kJ/kg	$\omega = 0.28$ C $= 0.6558$ GPa	$\omega = 0.11$ C $= 1.2160$ GPa
	$Q_c = 7590$ kJ/kg		

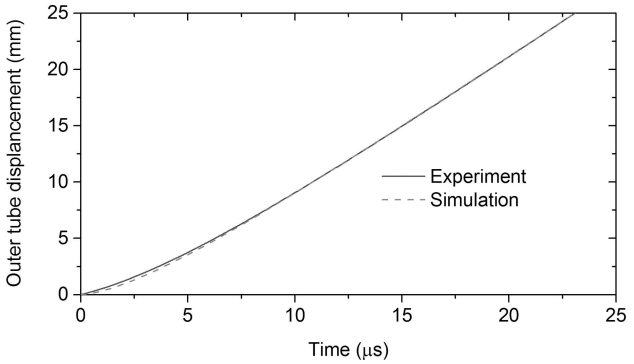

Figure 7. Experimental and calculated profiles of the copper tube driven by the detonation products of BH (E_0 equal to the detonation energy).

nation products during their expansion in the case of free charges or light cased charges, and on the other hand, the JWL EOS obtained for the detonation energy equivalent to the calorimetric heat describes better the expansion of the products after the detonation of the composite charge placed in a heavy casing.

6 Conclusions

The detonation characteristics of a novel aluminized explosive added with B and MgH_2 (BH) were studied in this work. Compared with a similar formulated aluminized explosive (AL), BH has a slightly higher calorimetric heat of explosion. The detonation pressure is almost the same for both explosives within the experimental error. The tube total velocity and Gurney energy of AL are higher than those of BH at a relative volume of detonation products of nine, however, the profiles of AL and BH both undergo an upward trend during the relative volume of detonation products expanding from 3 to 10, indicating the persisting energy output and a remained amount of energy is still stored in the detonation products. Moreover, the slope of BH is steeper than that of AL at the later expanding process of cylinder tube, which exhibits a stronger afterburning effect of BH. Finally, the JWL isentrope of these two explosives were determined from the cylinder test results using different detonation energy E_0. The JWL EOS used to describe the physical properties of the detonation products should be different according to the casing conditions.

In view of the higher calorimetric heat of explosion and remained amount of energy of the aluminized explosive added with B and MgH_2, further research needs to be conducted to study the energy output of it at a longer time scale (e.g. underwater explosion, confined explosion), which may exhibit the potential afterburning effects better.

Acknowledgements

This research is supported by the National Natural Science Foundation of China (11602238, 11572359, 11702265).

References

[1] P. P. Vadhe, R. B. Pawar, R. K. Sinha, S. N. Asthana, A. Subhananda Rao, Cast aluminized explosives (review), *Combust. Explos. Shock Waves* **2008**, *44*, 461–477.
[2] N. H. Yen, L. Y. Wang, Reactive Metals in Explosives, *Propellants Explos. Pyrotech.* **2012**, *37*, 143–155.
[3] A. Ulas, K. K. Kuo, C. Gotzmer, Ignition and combustion of boron particles in fluorine-containing environments, *Combust. Flame* **2001**, *127*, 1935–1957.
[4] C. L. Yeh, K. K. Kuo, Ignition and combustion of boron particles, *Prog. Energy Combust. Sci.* **1996**, *22*, 511–541.
[5] M. N. Makhov, Effect of aluminum and boron additives on the heat of explosion and acceleration ability of high explosives, *Russ. J. Phys. Chem. B* **2015**, *9*, 50–55.
[6] S. Xu, Y. Chen, X. Chen, D. Wu, D. Liu, Combustion heat of the Al/B powder and its application in metallized explosives in underwater explosions, *Combust. Explos. Shock Waves* **2016**, *52*, 342–349.
[7] Y. Chen, X. Chen, D. Wu, S. Xu, D. Liu, M. Xu, Underwater Explosion Analysis of Hexogen-Enriched Novel Hydrogen Storage Alloy, *J. Energ. Mater.* **2016**, *34*, 49–61.
[8] H. Krier, R. L. Burton, S. R. Pirman, M. J. Spalding, Shock initiation of crystalline boron in oxygen and fluorine compounds, *J. Propul. Power* **1996**, *12*, 672–679.

 © 2019 Wiley-VCH Verlag GmbH & Co. KGaA, Weinheim

[9] T. Yoshida, S. Yuasa, Effect of water vapor on ignition and combustion of boron lumps in an oxygen stream, *Proc. Combust. Inst.* **2000**, *28*, 2735–2741.
[10] B. Sakintuna, F. Lamari-Darkrim, M. Hirscher, Metal hydride materials for solid hydrogen storage: A review, *Int. J. Hydrogen Energy* **2007**, *32*, 1121–1140.
[11] A. A. Selezenev, V. N. Lashkov, V. N. Lobanov, O. L. Ignatov, A. Y. Aleinikov, A. V. Strikanov, V. N. Trusov, *Effect of Al/AlH$_3$ and Mg/MgH$_2$ components on detonation parameters of mixed explosives*, 12th International Detonation Symposium, San Diego, California, USA, 11–16 August, **2002**, p. 741–744.
[12] B. Xue, H.-H. Ma, Z.-W. Shen, Air explosion characteristics of a novel TiH$_2$/RDX composite explosive, *Combust. Explos. Shock Waves* **2015**, *51*, 488–494.
[13] B. Xue, H. Ma, Z. Shen, L. Ren, M. Lin, Effect of TiH$_2$ Particle Size and Content on the Underwater Explosion Performance of RDX-Based Explosives, *Propellants Explos. Pyrotech.* **2017**, *42*, 791–798.
[14] B. Xue, M. Lin, H. Ma, Y. Wang, Z. Shen, Energy Performance and Aging of RDX-based TiH$_2$, MgH$_2$ Explosive Composites, *Propellants Explos. Pyrotech.* **2018**, *43*, 671–678.
[15] Y. F. Cheng, H. H. Ma, Z. W. Shen, Detonation characteristics of emulsion explosives sensitized by MgH$_2$, *Combust. Explos. Shock Waves* **2013**, *49*, 614–619.
[16] Y. Cheng, H. Ma, R. Liu, Z. Shen, Explosion Power and Pressure Desensitization Resisting Property of Emulsion Explosives Sensitized by MgH$_2$, *J. Energ. Mater.* **2014**, *32*, 207–218.
[17] Y.-F. Cheng, X.-R. Meng, C.-T. Feng, Q. Wang, S.-S. Wu, H.-H. Ma, Z.-W. Shen, The Effect of the Hydrogen Containing Material TiH$_2$ on the Detonation Characteristics of Emulsion Explosives, *Propellants Explos. Pyrotech.* **2017**, *42*, 585–591.
[18] S. Cudziło, W. A. Trzciński, J. Paszula, M. Szala, Z. Chyłek, Effect of Titanium and Zirconium Hydrides on the Detonation Heat of RDX-based Explosives – A Comparison to Aluminium, *Propellants Explos. Pyrotech.* **2018**, *43*, 280–285.
[19] S. Cudziło, W. A. Trzciński, J. Paszula, M. Szala, Z. Chyłek, Effect of Titanium and Zirconium Hydrides on the Parameters of Confined Explosions of RDX-Based Explosives – A Comparison to Aluminium, *Propellants Explos. Pyrotech.* **2018**, *43*, 1048–1055
[20] M. Yao, W. Ding, G. Rao, L. Chen, J. Peng, Effects of MgH$_2$/Mg(BH$_4$)$_2$ Powders on the Mechanical Sensitivity of Conventional Explosive Compounds, *Propellants Explos. Pyrotech.* **2018**, *43*, 274–279.
[21] M. Yao, L. Chen, J. Peng, Effects of MgH$_2$/Mg(BH$_4$)$_2$ Powders on the Thermal Decomposition Behaviors of 2,4,6-Trinitrotoluene (TNT), *Propellants Explos. Pyrotech.* **2015**, *40*, 197–202.
[22] Y. Yue, L. Chen, J. Peng, Thermal Behaviors and Their Correlations of Mg(BH$_4$)$_2$-Contained Explosives, *J. Energ. Mater.* **2018**, *36*, 82–92.
[23] D. Ornellas, *Calorimetric determinations of the heat and products of detonation for explosives: October 1961 to April 1982*, Report No. UCRL-52821, Lawrence Livermore National Laboratory, **1982**.
[24] X. Guo, Y. Han, Y. Wen, K. Tan, W. Cao, Experimental Study on Head-on Collisions of Detonation Waves in Insensitive High Explosive, *Sci. Technol. Energ. Mater.* **2019**, *80*, 46–49.
[25] P. A. Rigg, M. D. Knudson, R. J. Scharff, R. S. Hixson, Determining the refractive index of shocked [100] lithium fluoride to the limit of transmissibility, *J. Appl. Phys.* **2014**, *116*, 033515.
[26] R. E. Duff, E. Houston, Measurement of the Chapman-Jouguet Pressure and Reaction Zone Length in a Detonating High Explosive, *J. Chem. Phys.* **1955**, *23*, 1268–1273.
[27] Q. Liu, X. Zhou, X. Zeng, S. N. Luo, Sound velocity, equation of state, temperature and melting of LiF single crystals under shock compression, *J. Appl. Phys.* **2015**, *117*, 045901.
[28] J. K. Rigdon, I. B. Akst, An analysis of the "aquarium technique" as a precision detonation pressure measurement gage, *5th Symposium (International) on Detonation*, Pasadena, California, USA, **1970**, p. 59–66.
[29] W. A. Trzciński, L. Szymańczyk, B. Kramarczyk, Determination of the Equation of State for the Detonation Products of Emulsion Explosives, *Cent. Eur. J. Energ. Mater.* **2019**, *16*, 49–64.
[30] H. Hornberg, Determination of Fume State Parameters from Expansion Measurements of Metal Tubes, *Propellants Explos. Pyrotech.* **1986**, *11*, 23–31.
[31] H. Hornberg, F. Volk, The cylinder test in the context of physical detonation measurement methods, *Propellants Explos. Pyrotech.* **1989**, *14*, 199–211.
[32] L. Maiz, W. A. Trzciński, Detonation Characteristics of New Aluminized Enhanced Blast Composites, *Propellants Explos. Pyrotech.* **2018**, *43*, 650–656.
[33] W. A. Trzciński, S. Cudziło, L. Szymańczyk, Studies of Detonation Characteristics of Aluminum Enriched RDX Compositions, *Propellants Explos. Pyrotech.* **2007**, *32*, 392–400.
[34] E. Lee, H. Hornig, J. Kury, *Adiabatic expansion of high explosive detonation products*, Report No. UCRL-50422, Lawrence Livermore National Laboratory, **1968**.
[35] *LS-DYNA keyword user's manual*, Livermore Software Technology Corporation, **2007**.
[36] C. E. Needham, *Blast Waves*, Springer, New York **2010**, p. 304.

Manuscript received: May 18, 2019
Revised manuscript received: July 4, 2019
Version of record online: July 26, 2019

 © 2019 Wiley-VCH Verlag GmbH & Co. KGaA, Weinheim